2011 APR 24

Liquid-Air Transpired Solar Collector: Model Development and Sensitivity Analysis

Abdul Qadir
Graduate Student, Masdar Institute of Science and Technology
Abu Dhabi, United Arab Emirates

Peter R. Armstrong
Associate Professor, Masdar Institute of Science and Technology
Abu Dhabi, United Arab Emirates

ABSTRACT

The paper develops a numerical model of a novel hybrid liquid-air transpired solar collector which simultaneously heats air and water. An energy balance is performed on an absorber plate element, leading to a system of ODEs which is integrated to obtain the air and water outlet temperatures of the collector. Three sets of sensitivity analyses have been performed on the collector by varying total thermal capacitance rate of air and water $(\dot{m}c_p)_{total}$, ratio of air capacitance rate to total capacitance rate $R_{\dot{m}cp}$, water inlet temperature T_{wi}, ambient temperature T_{amb}, solar radiation G, and wind speed V_w. General performance curves for the collector with increasing $(T_{wi}-T_{amb})/G$ have been developed as a result of these analyses. It is noticed that values of $R_{\dot{m}cp}$ between 0.5 and 0.6 provide the highest collector performance. At low $R_{\dot{m}cp}$, collector performance becomes sensitive to wind speed. The Hottel-Whillier equation is shown to be a reasonable approximation for the collector when the radiation loss term is linearized, U_L is evaluated for a specific wind condition, and the perforations are optimized for maximum heating of water.

INTRODUCTION

Over 60% of peak electricity usage in Abu Dhabi city is attributed to cooling[1]. This, coupled with the high solar resource[2], encourages the use of solar energy towards cooling applications. The city of Abu Dhabi has a very humid climate, where summer time humidity ratios go up to 25.2 g/kg[2]. It has been proposed that latent loads can be economically addressed by thermally regenerated desiccant cycles[3]. This allows for the separation of latent and sensible cooling functions and thus higher chilled water temperatures may be used to handle the sensible cooling load, decreasing the energy input to a vapor compression chiller[4]. Moreover absorption chillers designed to operate at higher chilled water temperatures can also have higher COP than those operating at lower chilled water temperatures[3].

Solar energy can be used to regenerate liquid desiccants and some of the regenerated liquid can be stored for use at night. Previously studies have considered the use of flat plate collectors and transpired solar collectors in desiccant regeneration applications[5]. However the use of both glazed and unglazed flat plate water heating collectors as well as transpired collectors has proved economically unfeasible [6]. Regenerators powered only by hot air are not very efficient and unglazed liquid collectors exhibit low efficiencies when heating water to a regeneration temperature of 70°C while glazed flat plate collectors have higher efficiencies but are significantly more expensive. There have also been efforts in the past towards developing a low cost unglazed solar collector for domestic water heating[7, 8].

This paper formulates the steady state model of a potentially economical and efficient unglazed, liquid-air transpired solar collector (LATSC) that simultaneously heats water and ambient air. We postulate that this type of collector could be especially useful for desiccant regeneration because the regeneration process needs a continuous supply of fresh air to carry away vapor released when the weak LiBr solution is heated moderately to a temperature below its bubble point. Thus the heat gain of the LATSC suction air (whose main purpose in this application is suppression of convection loss) can be put to good use in the desiccant regeneration process.

Using a steady-state finite difference model we explore the sensitivity of LATSC collection efficiency to variations in air and water flow rate, water inlet temperature, and ambient conditions of temperature, incident solar irradiation, and wind speed.

NOMENCLATURE

A_c	Area (m^2)
c_{pa}	Specific heat of air (kJ/kgK)
c_{pw}	Specific heat of water (kJ/kgK)
D_h	Hole diameter (m)

D_p Hydraulic diameter of plenum (m)
D_t Tube diameter (m)
ε_{hx} Heat exchange effectiveness of perforated plate
F Fin efficiency
F_{cs} Collector view factor with sky
F_{cg} Collector view factor with ground
F' Plate efficiency factor
F_R Collector heat removal factor for water
G Absorbed solar radiation (W/m^2)
h_{fi} Heat transfer coefficient inside tubes (W/m^{2}K)
k Thermal conductivity (W/mK)
L Length of collector (m)
L_c Characteristic length of collector (m)
$(\dot{m}c_p)_{total}$ Total thermal capacitance rate of air and water
$\dot{m}_a$ Mass flow rate (kg/s)
$R_{\dot{m}cp}$ Ratio of $\dot{m}c_{p_{air}}$ to $\dot{m}c_{p_{total}}$
Nu Nusselt number
NTU Number of transfer units
P Perimeter of plenum cross section (m)
$Pitch$ Spacing of holes on absorber plate (m)
por Plate porosity
q_{back} Convection to air in back channel per unit area(W/m^2)
$q_{back,loss}$ Back convection loss per unit area(W/m^2)
$q_{conv,loss}$ Convection loss per unit area(W/m^2)
$q_{rad,loss}$ Radiation loss per unit area (W/m^2)
$q_{c,air}$ Heat transferred to suction air per unit area (W/m^2)
Q_u Useful energy transferred to water (W)
Re Reynolds Number
sep Distance between tubes in absorber
t Thickness (m)
T_a(y) Air temperature (K)
T_{amb} Ambient temperature (K)
T_{fm} Local fluid mean temperature (K)
T_m(y) Mean of plate and sky temperature (K)
T_{pl}(y) Plate temperature (K)
T_{sky} Sky Temperature (K)
T_w(y) Water Temperature (K)
U Heat transfer coefficient (W/m^{2}K)
V_s Suction face velocity
V_w Wind Speed
W Width of collector (m)
x lateral distance from tube
y distance from inlet end of collector

Greek letters:

α plate absorptivity
β Collector Inclination
δ Plate thickness (m)
ϵ Emissivity of collector plate
ρ Density (kg/m^3)
ν Kinematic viscosity (m^2/s)
σ Stephan-Boltzmann constant

Subscripts:

a air
ab back of absorber plate
bi back insulation
bp back plate
br back of absorber plate radiation
c collector
d pertaining to air flowing through perforations
e edge of plate
exit exit from the perforations
i inlet
o outlet
p plate
tot air +water
w water
windb pertaining to wind at back of collector
windf pertaining to wind at front of collector

MODEL FORMULATION

The collector profile is that of a fin tube flat plate collector in which the plate used is perforated in the manner of a conventional transpired solar collector [9, 10]. Thus water is heated in tubes that run from the base of the collector to the top where it exits via a standard header tube, while the air is sucked through the plate and heated as it travels behind the plate from a given point of entry to the top where it exits via an air duct. A schematic cross-section looking upstream is shown in Figure 1.

The energy balance on a unit-width differential element of the collector is shown in figure 2.

The energy balances for water and air respectively are:

$$\dot{m}_w c_{pw} \frac{dT_w}{dy} = Q_u \quad (1)$$

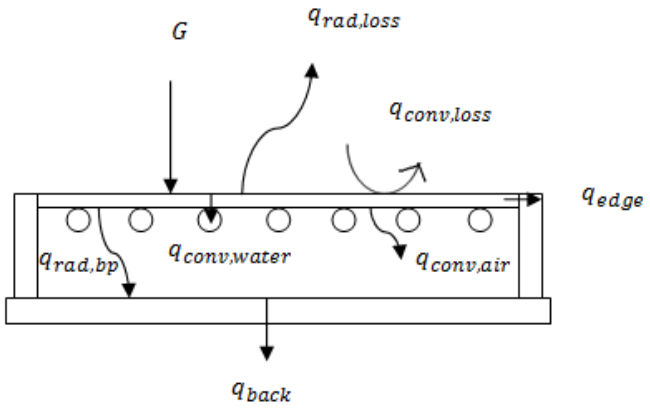

Figure 1: Cross-section of collector looking upstream

$$(\dot{m}_{ai} + \Delta\dot{m}_a)\frac{dT_a}{dy} = \frac{\dot{m}_{a,tot}}{L}[(1 - e_{hx})T_{amb} + e_{hx}T_{pl} - T_{ai}] \quad (2)$$

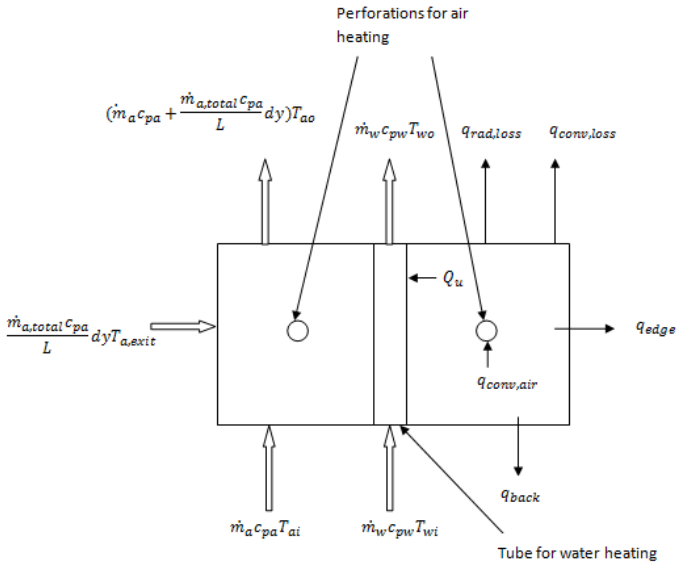

Figure 2: Differential element of the collector in plan view

The mass balance for air entering each element of the collector is:

$$\frac{d\dot{m}_a}{dy} = \frac{\dot{m}_{a,total}(y)}{L} \tag{3}$$

The expressions for ε_{hx} and Q_u are developed below.
In the above expressions, ε_{hx} is the heat exchange effectiveness of the perforated plate and is calculated by the following correlations developed in literature[9]:

$$Re_d = \frac{V_s D_h}{por * v_a} \tag{4}$$

$$Nu_d = 2.75\left(\left(\frac{pitch}{D_h}\right)^{-1.21} {Re_d}^{0.43} + 0.011 por * Re_d \left(\frac{V_w}{V_s}\right)^{0.48}\right) \tag{5}$$

$$U_d = \frac{Nu_d k_a}{D_h} \tag{6}$$

$$V_s = \frac{\dot{m}_a}{\rho_a A(1-\frac{D_t}{sep})} \tag{7}$$

$$NTU = \frac{U_d(1-por)}{\rho_a V_s c_{pa}} \tag{8}$$

$$e_{hx} = 1 - \exp(-NTU) \tag{9}$$

Furthermore we require the plate temperature T_{pl} and heat transferred to the water Q_u in order to solve the derived ODEs. In order to obtain these we account for the convective and radiative heat losses from the top and bottom of the plate as well as edge losses.

Firstly we tackle the top convective heat loss due to wind which is sensitive to air face velocity according to:

$$q_{conv,loss} = U_{wf}(T_{pl} - T_{amb})) \tag{10}$$

where,

$$U_{wf} = 0.82 \frac{V_w v_a \rho_a c_{pa}}{V_s L} \tag{11}$$

Then we account for the top heat loss due to radiation:

$$q_{rad,loss} = \epsilon\sigma({T_{pl}}^4 - F_{cs}{T_{sky}}^4 - F_{cg}{T_g}^4) \tag{12}$$

where F_{cs} and F_{cg} are the views factor of the collector to the sky and ground respectively. The sky temperature, T_{sky} is estimated using the sky model correlation developed by Martin and Berdahl[11]. The views factors will depend on the collector inclination β.

We can also express the heat transferred to the air as it passes through the perforations as a convective heat loss from the plate.

$$q_{c,air} = \dot{m}_a c_{pa} e_{hx} \frac{(T_{pl} - T_{amb})}{A_c} \tag{14}$$

The edge loss coefficient for heat loss from the absorber plate per unit area can be expressed as:

$$U_e = \frac{k_e}{t_e}\left(\frac{A_{edge}}{A_c}\right) \tag{15}$$

Lastly we will analyze the back losses from the collector plate. The back losses of the collector consists of the radiation from the back of the absorber plate to the back plate, followed by heat conduction through the back insulation to the collector back and heat loss at the back of the collector through convection and radiation. The radiation heat transfer coefficient for heat transfer between the absorber plate and back plate is given by [12]:

$$U_{br} = \frac{\sigma({T_{pl}}^4 - {T_{bp}}^4)}{\frac{1}{\epsilon_{ab}} + \frac{1}{\epsilon_{bp}} - 1} \tag{16}$$

where T_{bp} is the back plate temperature and ϵ_{ab} and ϵ_{bp} are the back of the absorber plate and front of the back plate emissivities respectively.

The heat transfer coefficient for conduction through the back insulation is given by:

$$U_{bi} = \frac{k_{bi}}{t_{bi}} \tag{17}$$

Furthermore the convective heat transfer coefficient at the back of the collector is given by:

$$U_{wb} = \frac{Nu_{wb} k_a}{W} \tag{18}$$

where:

$$Re_{wb} = \frac{V_w W}{\nu_a} \tag{19}$$

$$Nu_{wb} = 0.664\left(Re_{wb}{}^{0.5} * Pr_{wb}{}^{0.33}\right) \tag{20}$$

The radiative heat transfer convection for radiation at the back of the collector to the ground is:

$$U_{br} = \frac{\sigma\left(T_{bc}{}^2 + T_g{}^2\right)+\left(T_{bc}+T_g\right)}{\frac{1}{\epsilon_{bc}}+\frac{1}{\epsilon_g}-1} \tag{21}$$

where T_g is the ground temperature and it is approximated to be the ambient temperature. ϵ_{bc} and ϵ_g are the collector back and ground emissivities.

The total heat transfer at the back of the collector is:

$$q_{back,loss} = U_{wb}(T_{bc} - T_{amb}) + U_{br}\left(T_{bc} - T_g\right) \tag{22}$$

Thus the overall heat transfer coefficient from the back of the absorber plate can be expressed as:

$$U_l = \frac{q_{rad,loss}+q_{c,air}+q_{conv,loss}+q_{back,loss}}{(T_{pl}-T_{amb})} + U_e \tag{23}$$

The first term on the right hand side of the equation (23) is the combined top and back loss coefficient while the second term is the edge loss coefficient.

We can now write an expression for the total energy transferred to the water at each element by performing an energy balance on that element using U_l[13].

$$Q_u = W * dy * (G\alpha - U_l\left(T_{pl} - T_{amb}\right)) \tag{24}$$

As the plate temperature varies in both the x and y direction, it is useful to express Q_u in terms of the local mean fluid temperature T_{fm}:

$$Q_u = W * dy * F'(G\alpha - U_l\left(T_{fm} - T_{amb}\right)) \tag{25}$$

Where F' is the collector efficiency factor which accounts for thermal resistances between various points on the plate and the cooling water. Part of the resistance is due to fin efficiency, F, of the collector plate. These factors are given by:

$$F' = \frac{\frac{1}{U_l}}{sep\left(\frac{1}{U_l(D_t+(sep-D_t)F)}+\frac{1}{C_b}+\frac{1}{\pi D_t h_{fi}}\right)} \tag{26}$$

where

$$F = \frac{tanh * m\frac{sep-D_t}{2}}{m\frac{sep-D_t}{2}} \tag{27}$$

and

$$m = \sqrt{\frac{U_l}{k_p \delta}} \tag{28}$$

Uncoupled Model

The model derived so far does not take in to account the heating of air behind the collector plate as the air moves up the collector towards the outlet. We call this the uncoupled model. In this model, for a finite air flow rate, a uniformly porous plate will produce a laminar boundary layer that is continuously replenished from the plate and thus completely suppresses convective coupling with the cooler air that is already moving through the channel.

Figure 3 demonstrates the flow of air behind the collector with the injection of air in to the airstream due to the suction at the front side of the collector plate. Figure 3(a) illustrates the case of the uncoupled model while Figure 3(b) shows the case of the coupled model.

The uncoupled model provides a lower limit for the air outlet temperature and upper limit of the water outlet temperature.

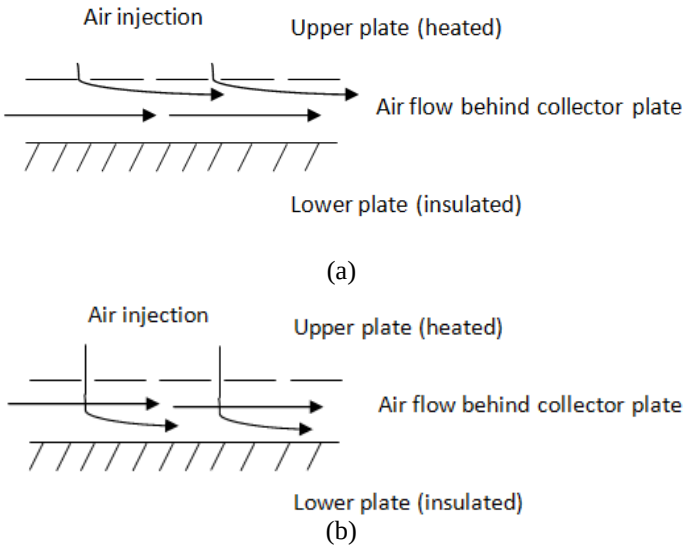

Figure 3: Air flow behind the collector plate: (a) for uncoupled flow, (b) for coupled flow

Coupled Model

On the other hand if it is assumed that there is no boundary layer replenishment by air through the plate and that the flow behind the collector is laminar with uniform heat flux from the plate and the back wall insulated, we can obtain a model which will provide the upper limit of the air outlet temperature and lower limit of the water outlet temperature. In order to accurately calculate the heating of the air behind the plate (coupled heating) a correlation is needed which accounts for the fact that while the air behind the plate has some contact with the plate, there is also an injection of air through the plate which may limit complete contact with the plate. For this model

it is assumed that the air flowing behind the collector is laminar and the width of the collector is considerably larger than the plenum depth. The Nusselt number for such a flow is 5.39[12]. Thus U_{ab} is calculated as:

$$U_{ab} = \frac{Nu_{bp}k_a}{D_p} \quad (29)$$

where

$$D_p = \frac{4A_c}{P} \quad (30)$$

The heat transferred to the air behind the collector is thus:

$$q_{back} = U_{ab} * (T_{pl} - T_{ai}) \quad (31)$$

For the uncoupled model, the 'loss' term of (23) is added to the numerator in equation (15) to account for the heat extracted from the plate. Furthermore q_{back} is also added to the right hand side of equation (2) in order to obtain the energy balance for the air.

The two energy balance equations (1&2) and the mass balance equation (3) were then solved simultaneously using the fourth/fifth order Runge-Kutta method in the computation software Matlab™[14].
Thus by solving these equations, the outlet air and water temperature through the collector and consequently the efficiency of the collector are obtained for the models with and without heating of the air behind the collector plate. The efficiency of the collector is given by:

$$\eta_{coll} = \frac{\dot{m}_a c_{pa}*(T_{ao}-T_{ai})+\dot{m}_w c_{pw}*(T_{wo}-T_{wi})}{G*A_c} \quad (32)$$

SENSITIVITY ANALYSIS

With the foregoing collector model we can observe the performance sensitivity of the collector to varying the ambient temperature(T_{amb}), inlet water temperature(T_{wi}), collector emissivity(ϵ) and total thermal capacitance of air and water($(\dot{m}c_p)_{total}=\dot{m}_w c_{pw} + \dot{m}_a c_{pa}$). Moreover for each analysis, the ratio of thermal capacitance of air to total thermal capacitance ($R_{\dot{m}cp}$) was varied to observe the effect it had on the efficiency of the collector along with the other varying parameters. Throughout the analysis, the collector dimension, air properties, weather condition and solar radiation have been held constant at values specified in Table 1.

The first analysis was aimed at obtaining the performance of the collector with different $(\dot{m}c_p)_{total}$ entering the collector along with a range of values of $R_{\dot{m}cp}$ from 0.1 to 0.9. The range of values of $(\dot{m}c_p)_{total}$ was from 5W/m^{2}K to 25W/m^{2}K at five equal intervals and the ambient temperature was maintained at =25^{o}C. The results obtained for these analyses are shown in figure 4 and 6 for the model without heating the air behind the collector plate and in figure 5 and 7 when air is heated behind the collector plate.

Table1: Geometric parameters, fluid properties and baseline conditions used in the sensitivity analysis

Property	**Value**
Solar radiation (G)	800W/m^2
Collector Inclination (β)	0^o
Wind speed(V_w)	3 m/s
Air temperature(T_{amb})	25 °C
Air density(ρ_a)	1.184kg/m^3
Air Viscosity (μ_a)	1.849*10^{-5} Ns/m^2
Air Thermal Capacitance (c_{pa})	1.007kJ/kgK
Length of collector (L)	2m
Width of collector (W)	1m
Plenum depth (D)	0.1m
Perimeter of plenum cross section	2.2m
Plate absorptivity	0.9
Plate emissivity	0.9
Hole diameter	0.00159m
Hole pitch (triangular pattern)	0.025m

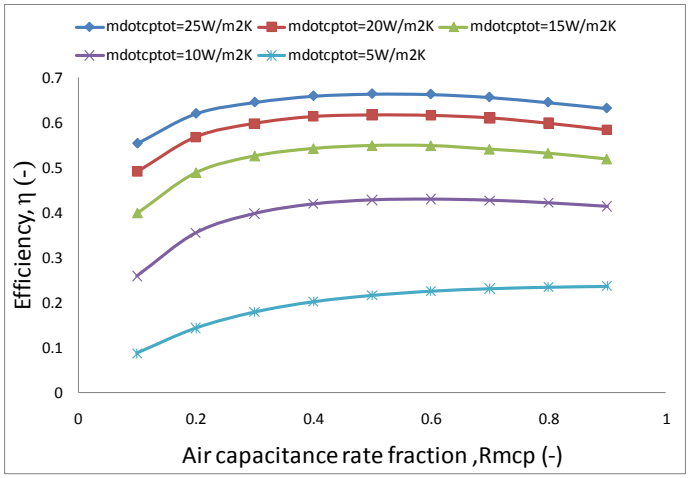

Figure 4: Efficiency vs. $R_{\dot{m}cp}$ for range of $(\dot{m}c_p)_{total}$ with $T_{w,i}$ = T_{amb} = 25°C uncoupled air heating.

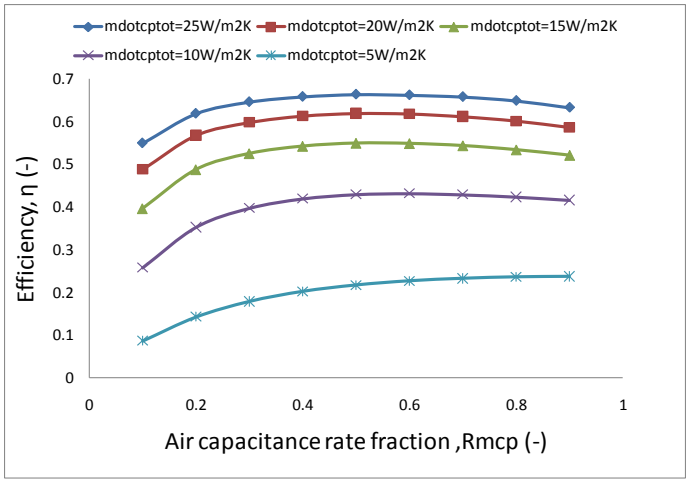

Figure 5: Efficiency vs. $R_{\dot{m}cp}$ for range of $(\dot{m}c_p)_{total}$ with $T_{w,i}$ = T_{amb} = 25°C for coupled air heating.

The second set of analysis was performed by varying the inlet temperature of the water from 25°C to 115°C to obtain the efficiency of the collector. The ambient temperature for this analysis was fixed at 25°C and the $(\dot{m}c_p)_{total}$ was fixed at 15W/m^{2}K. The emissivity and $R_{\dot{m}cp}$ were also varied to obtain families of curves for emissivity = 0.1, 0.5 and 0.9 and for $R_{\dot{m}cp}$ = 0.1, 0.5 and 0.9. The results are shown in figures 8, 9 and 10 respectively.

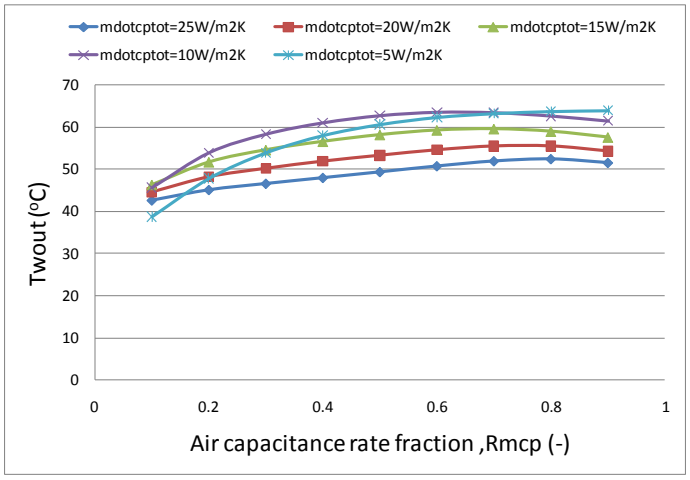

Figure 6: Water outlet temperature vs. $R_{\dot{m}cp}$ for range of $(\dot{m}c_p)_{total}$ with $T_{w,i}$ = T_{amb} = 25°C for uncoupled air heating.

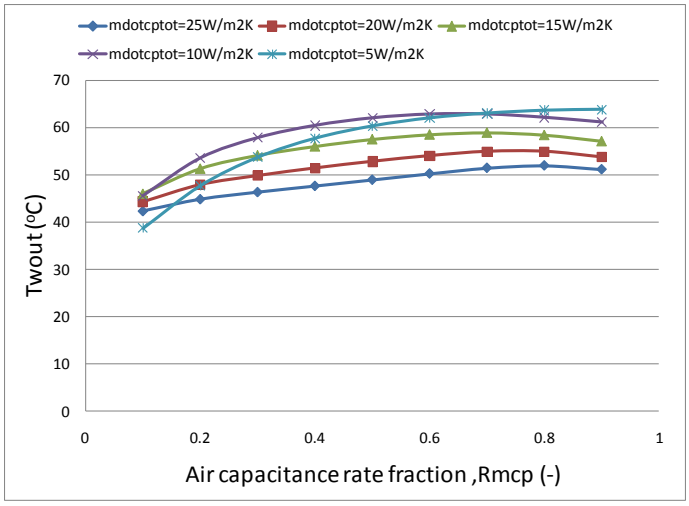

Figure 7: Water outlet temperature vs. $R_{\dot{m}cp}$ for range of $(\dot{m}c_p)_{total}$ with $T_{w,i}$ = T_{amb} = 25°C for coupled air heating.

The third analysis develops standard performance curves for the collector for a wider range of varying parameters and conditions. For this analysis $(\dot{m}c_p)_{total}$ has been kept constant at 15W/m^{2}K , while $R_{\dot{m}cp}$, V_w, T_{wi}, T_{amb} and $\underline{G}$ have been varied. The ranges of values for which these parameters have been varied are displayed in Table 2. The results from this analysis are illustrated in Figures 11-12 for uncoupled air heating and Figures 13-14 for coupled air heating behind the collector plate.

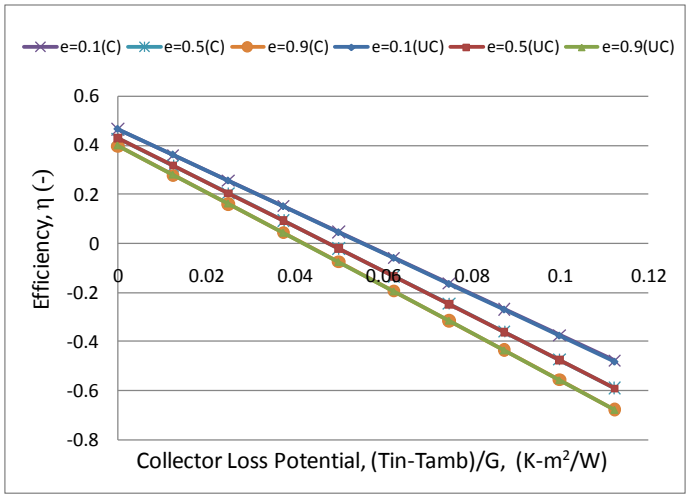

Figure 8: Efficiency vs. $\Delta T/G$ for $R_{\dot{m}cp}$= 0.1 and T_{amb} = 25°C for uncoupled (UC) and coupled(C) air heating behind plate.

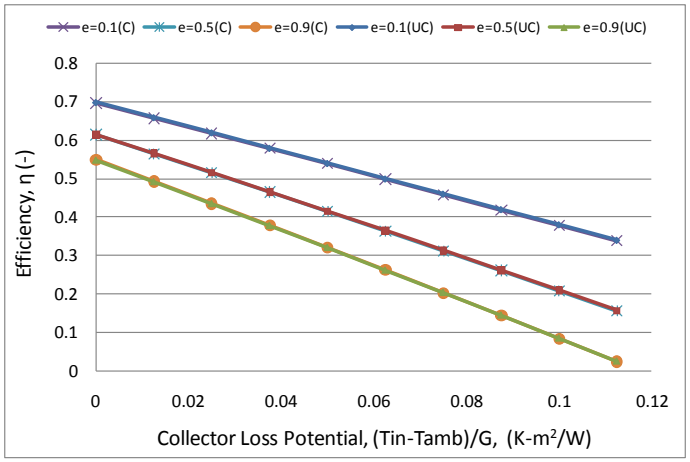

Figure 9: Efficiency vs. $\Delta T/G$ for $R_{\dot{m}cp}$= 0.5 and T_{amb} = 25°C for uncoupled (UC) and coupled(C) air heating behind plate.

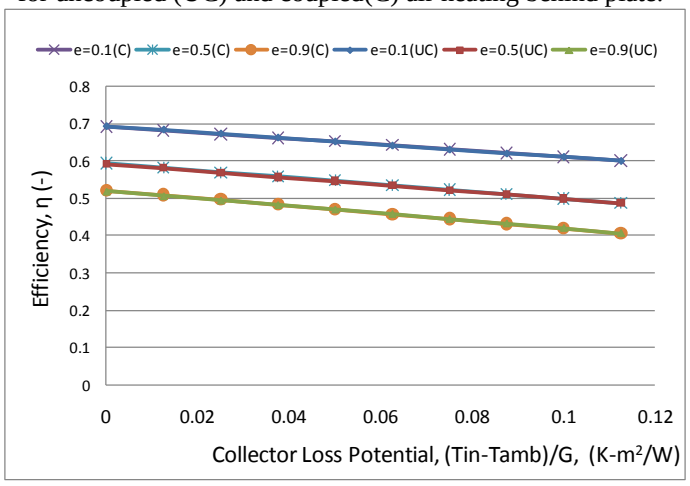

Figure 10: Efficiency vs. $\Delta T/G$ for $R_{\dot{m}cp}$= 0.9 and T_{amb} = 25°C for uncoupled (UC) and coupled(C) air heating behind plate.

Table 2: Conditions used in sensitivity analyses

Parameter	Values
[1]Air temperature (T_{amb})	25,35,45(°C)
[1]Water inlet temperature (T_{wi})	25-115 (°C) with 10 °C intervals
[1]Air to total thermal capacity ratio ($R_{\dot{m}cp}$)	0.1, 0.3, 0.5, 0.7, 0.9
[2]Solar radiation (G)	300, 500, 800 (W/m²)
[2]Wind speed (V_w)	0, 3, 5 (m/s)

(1) G and V_w are fixed for the first two sensitivity exercises at values given in Table 1.
(2) G and V_w are only varied for the standard collector performance curve plots (Figures 11-14) that show wind speed sensitivity.

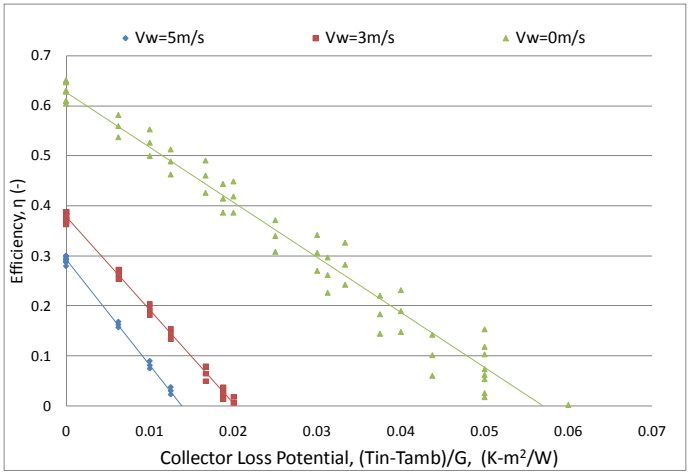

Figure 11: Efficiency vs. $\Delta T/G$ for $R_{\dot{m}cp}$= 0.1, $(\dot{m}c_p)_{total}$= 15W/m²K and varying G, T_{amb}, T_{win}, and V_w for uncoupled heating behind collector plate.

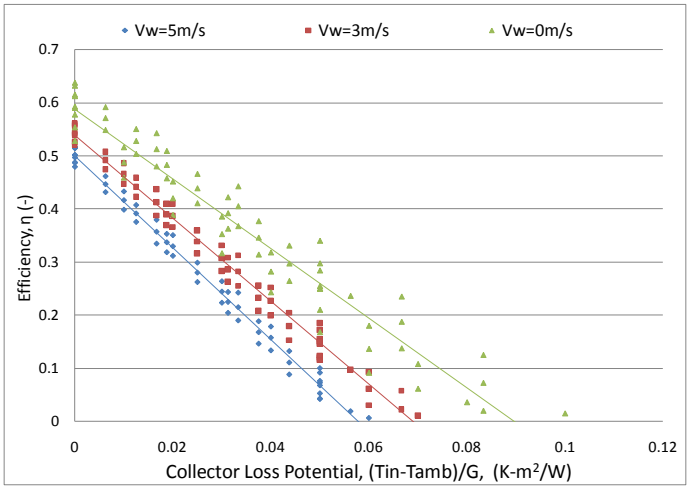

Figure 12: Efficiency vs. $\Delta T/G$ for $R_{\dot{m}cp}$ = 0.5, $(\dot{m}c_p)_{total}$= 15W/m²K and varying G, T_{amb}, T_{win}, and V_w for uncoupled heating behind collector plate.

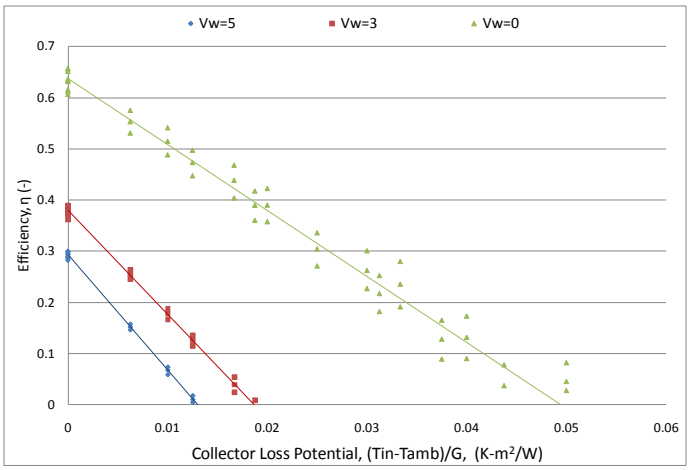

Figure 13: Efficiency vs. $\Delta T/G$ for $R_{\dot{m}cp}$ = 0.1, $(\dot{m}c_p)_{total}$ = 15W/m^{2}K and varying G, T_{amb}, T_{win}, and V_w with coupled heating behind collector plate.

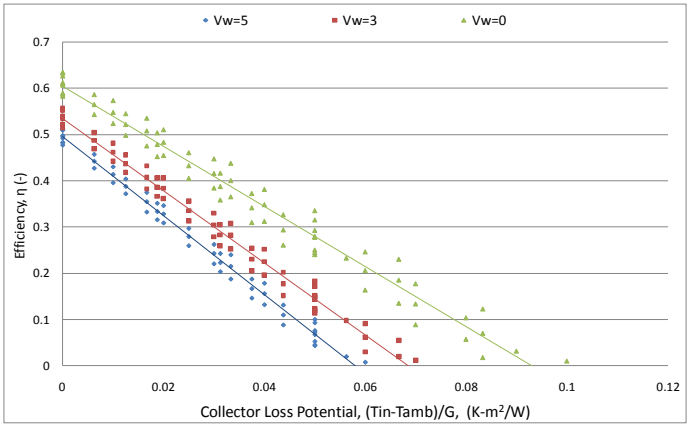

Figure 14: Efficiency vs. $\Delta T/G$ for $R_{\dot{m}cp}$= 0.5, $(\dot{m}c_p)_{total}$=15W/m^{2}K and varying G, T_{amb}, T_{win}, and V_w for coupled heating behind collector plate.

Finally the pitch and diameter of the holes was varied to assess the impact on the efficiency of the collector for the coupled model only. First the hole diameter was varied from 0.001 to 0.0055m, keeping the pitch constant at 0.025m. Then the hole diameter was kept constant at 0.00159m while the pitch was varied from 0.01 to 0.055m. This allowed for the collector performance to be simulated for a range of values of:

$$0.25 < \left(\frac{pitch}{D_h}\right)^{-1.21} Re_d{}^{0.43} < 1.039$$

This range lies within the range of values for which equation (5) is valid. The analysis was performed for total capacitance rates of 30, 40 and 50W/m^{2}K, keeping the air capacitance ratio of 0.5. The results of these analyses are shown in Figures 15 and 16 respectively.

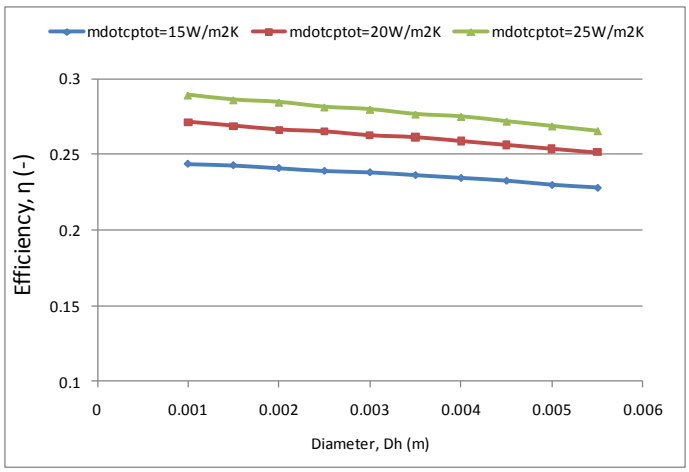

Figure 15: Efficiency vs. hole diameter for a constant pitch of 0.025m and air capacitance ratio of 0.5.

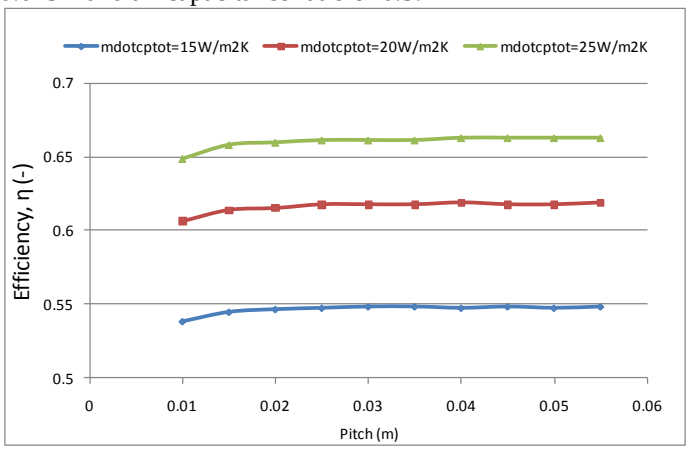

Figure 16: Efficiency vs. Pitch for a constant hole diameter of 0.00159m and air capacitance ratio of 0.5.

DISCUSSION

The results from the first sensitivity analysis show that the efficiency of the collector is highest when $R_{\dot{m}cp}$ is between 0.5 and 0.6 for both the uncoupled and coupled air heating model. It also shows the general trend of increasing efficiency with increasing$(\dot{m}c_p)_{total}$. The existence of a maximum efficiency point at an intermediate ratio of air-to-total flow rate may be attributed to the fact that as the $R_{\dot{m}cp}$ increases, the convective losses due to wind decrease, leading to an increase in the efficiency of the collector. However after a certain increase in $R_{\dot{m}cp}$, further increase in the ratio has very little effect on the convective losses. Thus as the mass flow rate of water decreases, the plate temperature increases, leading to a rapid increase in the radiative losses and, consequently, a decrease in collector efficiency.

As expected the collector is more efficient overall when heating of air behind the plate is promoted rather than suppressed. However the efficiency difference is not large as seen in figures

4 and 5. This means that if we design to suppress convective coupling behind the plate (e.g by using a denser pattern of smaller holes), the collector can be accurately modeled using the uncoupled model. One reason to suppress convection with as low an air flow rate as possible is to heat the water preferentially for the desiccant regeneration application. Another way to heat water preferentially, albeit with lower temperature rise, is to use high water flow rates as shown in Appendix 2.

The second sensitivity analysis shows the trend of decreasing efficiency of the collector for all three $R_{\dot{m}cp}$ of 0.1, 0.5 and 0.9 as $(T_i\text{-}T_{amb})/G$ is increased (Figures 7-12). One trend worth noticing is that as the $R_{\dot{m}cp}$ is increased, the decrease in efficiency with increasing $(T_i\text{-}T_{amb})/G$ is less steep. This can be attributed to the increased heat transfer to the air, which enters the collector at ambient temperature, with higher water inlet temperatures. The high flow rate of air through the collector prevents the plate from heating up too much, corresponding to low plate temperatures, which allows the collector to maintain a high efficiency at high inlet temperatures. This mode can be used in applications that can use more hot air than hot water.

The results from the third sensitivity analysis show that there is a general trend of decrease in the efficiency of the collector as $\Delta T/G$ is increased. The trend is highlighted by adding a line of best fit to the results obtained from the analysis. Furthermore it may be seen that when $R_{\dot{m}cp}$ is low (Figure 8), the efficiency of the collector is very sensitive to the wind speed. This phenomenon may be explained by the fact that at a low $R_{\dot{m}cp}$, the convective losses from the collector are weakly suppressed and thus an increase in the wind speed increases the convective losses with concomitant decrease in collector efficiency. It may be observed from Figure 9 ($R_{\dot{m}cp}$=0.5) that the LATSC behaves similar to a glazed collector. The designer must be mindful of local wind conditions when applying the same generalization to lower air capacitance ratios.

From the last sensitivity analysis, it may be seen that there is a general, but small, reduction in the efficiency of the collector with increase in hole diameter while there is a slight increase in efficiency with the increase in hole pitch.

FUTURE WORK

The next step in the study of the LATSC is experimental validation of the model. In this regard, a test rig based on a $2m^2$ collector has been assembled at MIST.
In addition to experimental verification a system model is being developed which integrates the LATSC and a liquid desiccant regeneration system to assess the performance of the regenerator coupled with the LATSC model. If the air flow ratio can be adjusted with relatively small adverse impact on the regeneration process, there is clearly an opportunity to maintain high overall efficiencies over a range of conditions by proper balancing of the air and water flow rates. The LATSC model must be linked to a regeneration process model for the control problem to be properly addressed.
In addition to the flow balance control problem, the opportunity to improve system performance by adjusting the distribution of collector plate porosity in the flow direction, currently modeled such that uniform face velocity is achieved, may be explored.

CONCLUSION

A numerical model of a novel hybrid liquid-air collector has been developed and the outlet water and air temperatures are evaluated by solving a system of ODEs. Two versions of the model are run: one with fully coupled heat transfer to the air behind the collector plate and the other with no heat transfer to the air behind the collector plate. Although the exact heat transfer situation behind the plate depends on plate perforation details, collector performance will always fall between the fully-coupled and uncoupled cases. The latter is shown to reduce to the Hottel-Whillier equation.

Key parameters of the model have been varied to assess the impact on the performance of the collector. Increasing the $(\dot{m}c_p)_{total}$ increases the efficiency of the collector for all values of $R_{\dot{m}cp}$. Moreover, an increase of the $R_{\dot{m}cp}$ from 0.1 to about 0.5 at a constant $(\dot{m}c_p)_{total}$ has shown to increase the efficiency of the collector while further increase in $R_{\dot{m}cp}$ has lead to a decrease in the efficiency because of higher plate temperatures near the outlet ends of the tubes. Furthermore, although an increase of $(T_i\text{-}T_{amb})/G$ always decreases the efficiency of the collector for $R_{\dot{m}cp}$ of 0.1, 0.5 and 0.9, the rate of decrease of the efficiency decreases with an increase in $R_{\dot{m}cp}$.

For a low $R_{\dot{m}cp}$ of 0.1, the efficiency of the collector exhibits considerable sensitivity to wind speed, showing that the convective losses are only marginally suppressed at low air flow rates. To heat the cooling water preferentially while still providing enough airflow to suppress convective front losses, it is desirable to conduct the air through the plate and into the airstream behind the plate in such a way that convective coupling is minimized.

REFERENCES

1. Ali, M.T., et al., *A Cooling Change-Point Model of Community-Aggregate Electrical Load.* Energy and Buildings, 2011. **43**: p. 28-37.
2. Remund, J., R. Lang, and S. Kunz, *METEONORM*. 2003, Meteotest: Bern, Switzerland.
3. Threlkeld, J.L., J.W. Ramsey, and T.H. Kuehn, *Thermal Environmental Engineering*. Third Edition. 1998: Prentice-Hall.
4. Armstrong, P.R., et al., *Efficient Low-Lift Cooling with Radiant Distribution, Thermal Storage, and Variable-*

Speed Chiller Controls— Part I: Component and Subsystem Models. HVAC&R RESEARCH, 2009. **15**(2): p. 366-400.
5. H.M Henning, T.E., C. Hindenburg, I.S. Santamaria, *The potential for solar energy use in desiccant cooling cycles* International Journal of Refrigeration, 2001. **24**: p. 220-229.
6. Pesaran, A.A. and K. Wipke, *Desiccant Cooling Using Unglazed Transpired Solar Collectors*, in *Solar '92*, S.M. Burley and M.E. Arden, Editors. 1992, American Solar Energy Society: Cocoa Beach Flordia.
7. Burch, J., et al., *Low-Cost Solar Domestic Hot Water Systems for Mild Climates*, D.o. Energy, Editor. 2005: Denver.
8. Burch, J., J. Salasovich, and T. Hillman, *An Assessment of Unglazed Solar Domestic Water Heaters*, in *ISES Soalr World Congress*. 2005: Orlando, Florida.
9. Kutscher, C.F., C.B. Christensen, and G.M. Barker, *Unglazed Transpired Solar Collectors: Heat Loss Theory.* Journal of Solar Energy Engineering, 1993. **115**(3): p. 182-188.
10. Kutscher, C.F., *Heat Exchange Effectiveness and Pressure Drop for Air Flow Through Perforated Plates With and Without Crosswind.* Journal of Heat Transfer, 1994. **116**(2): p. 391-399.
11. Martin, M. and P. Berdahl, *Characteristics of infrared sky radiation in the United States.* Solar Energy, 1984. **33**(3-4): p. 321-326.
12. Incropera, et al., *Fundamentals of Heat and Mass Transfer*. 2006: Wiley.
13. Duffie, J. and W. Beckman, *Solar Engineering of Thermal Processes*. 1980: John Wiley & Sons Inc.
14. *MATLAB*. 2008, The MathWorks, Inc.

APPENDIX 1:LINEARIZED MODEL OF UNCOUPLED CASE

We observed that the LATSC model with heat transfer to the air behind the absorber plate (coupled case) gives performance not much different from that given by the model with no heat transfer behind the absorber plate (uncoupled case). This observation suggests a simplified model based on the Hottel-Whillier (H-W) equation in which heating of the water is given by:

$$Q_u = A\left(F_R G - U_l\left(T_{fi} - T_{amb}\right)\right) \tag{33}$$

where:

$$F_R = \frac{\dot{m}_w c_{pw}}{A_c U_l F'}\left(1 - \exp\left(-\frac{A_c U_l F'}{\dot{m}_w c_{pw}}\right)\right) \tag{34}$$

F_R is the heat removal factor defined as the ratio of the rate of water heating to the heat rate that would occur if the plate temperature was equal to the fluid inlet temperature.

The H-W formulation requires a constant radiation heat transfer coefficient (h_r) with the sky temperature, T_{sky}, assumed to be equal to ambient temperature T_{amb}. Therefore equations 12 and 13 are changed to:

$$q_{rad,loss} = \epsilon\sigma 4{T_m}^3(T_{pl} - T_{amb}) \tag{35}$$

where

$$T_m = (T_{pl} + T_{amb})/2 \tag{36}$$

The radiation heat transfer coefficient of the plate can then be expressed as:

$$h_r = \epsilon\sigma 4{T_m}^3 \tag{37}$$

While the convective heat transfer coefficients due to wind and suction through the plate can be expressed as:

$$h_{wind} = 0.82\frac{V_w \nu_a \rho_a c_{pa}}{V_s L} \tag{38}$$

$$h_{c,air} = \dot{m}_a c_{pa} e_{hx} \tag{39}$$

The total heat loss coefficient from the plate is the sum of the three transfer coefficients for top loss and the back and edge loss coefficients:

$$U_l = h_r + h_{wind} + h_{c,air} + U_{b,tot} + U_e \tag{40}$$

where

$$U_{b,tot} = \frac{q_{back,loss}}{(T_{pl} - T_{amb})}$$

the air heating, which is not part of Q_u, is given by:

$$Q_{c,air} = \dot{m}_a c_{pa} \varepsilon_{hx}(T_{pm} - T_{amb}) \tag{41}$$

where

$$T_{pm} = T_{fi} + \frac{Q_u}{A_c F_R U_l}(1 - F_R) \tag{42}$$

The H-W model and the uncoupled form of the numerical model were simulated using identical inlet and ambient conditions and the linearized loss coefficients based on mean plate temperature (37-39). The results showed that both the air and water outlet temperatures match within the precision of MATLAB's numerical integrator ODE45.

Given reasonable initial estimates of h_r, h_{wind} and $h_{suction}$, one can expect to obtain an accurate estimate of T_{pl} and overall collector performance in two iterations.

APPENDIX 2: PERFORMANCE CURVES FOR THE COLLECTOR AT ASHRAE 93 STANDARD FLOW RATE.

The sensitivity analysis performed above is for low flow rate applications. In order to compare the LATSC with a conventional flat plate collector, the model was simulated at a water flow rate of 0.02 kg/s-m^2, which is used for the testing of water heating collectors specified by ASHRAE 93. This amounts to a water thermal capacitance rate of 83.5 W/m^2-K. First the optimum air flow rate was determined for maximum heat transfer to the water. For this, the water thermal capacitance rate was kept constant at 83.5W/m^2-K while the air thermal capacitance rate was varied from 0 to 20 W/m^2-K for wind speeds of 1m/s, 3m/s and 5m/s. The water heating efficiency, air heating efficiency and total efficiency of the collector with varying air flow rates is shown in figures 17-19.The air thermal capacitance rates at which the water heating efficiency was maximum was 2.5W/m^2-K, 5W/m^2-K and 6.5W/m^2-K (i.e R_{mcp} in the range .029~0.072) for wind speeds of 1m/s, 3m/s and 5m/s respectively.

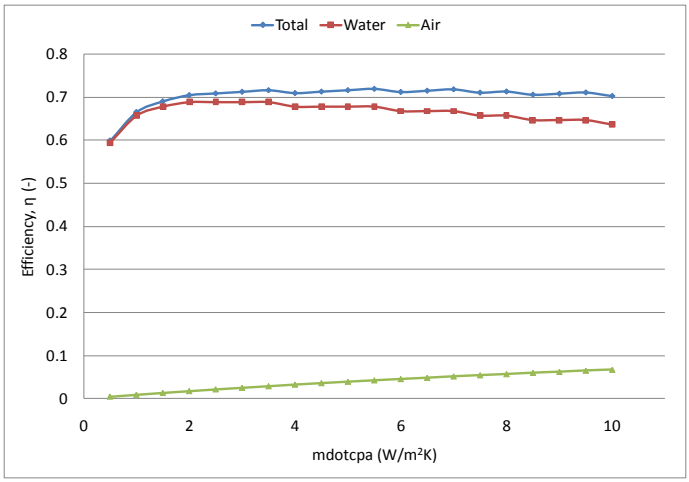

Figure 17: Air, Water and Total thermal efficiencies of the collector with increasing air flow rate at V_w=1m/s.

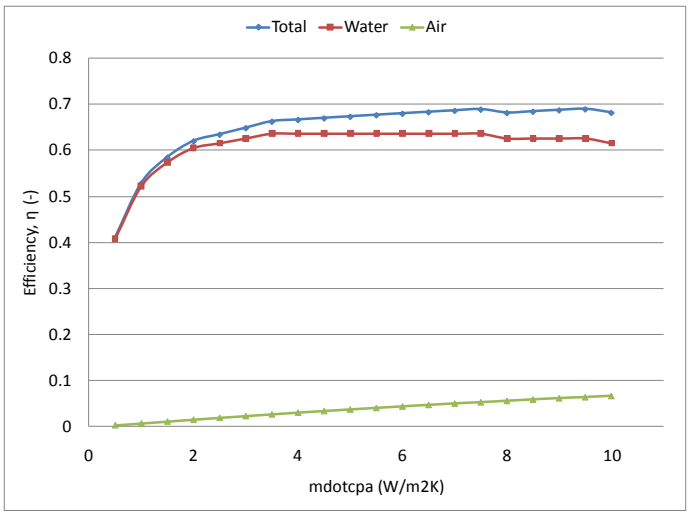

Figure 18: Air, Water and Total thermal efficiencies of the collector with increasing air flow rate at V_w=3m/s.

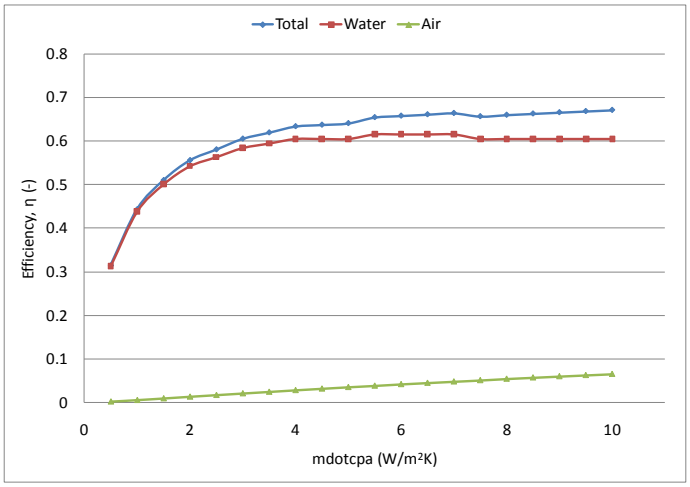

Figure 19: Air, Water and Total thermal efficiencies of the collector with increasing air flow rate at V_w=5m/s.

The collector was then simulated for wind speeds of 1m/s, 3m/s and 5m/s with their respective optimum air flow rates, varying the emissivity of the plate as well as the water inlet temperature. The input parameters for the model are those given in Table 1. The values for the inlet water temperature are those given in Table 2. Figures 20-22 show families of curves for the total efficiency of the collector for varying $(T_{in}-T_{amb})/G$ and plate emissivities. Figures 23-25 show the water heating efficiency of the LATSC for varying $(T_{in}-T_{amb})/G$ and plate emissivities.

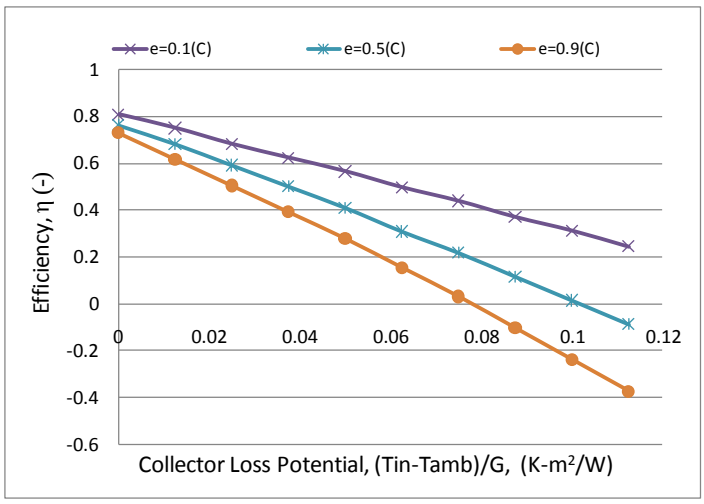

Figure 20: Total collector efficiency vs. ΔT/G at V_w=1m/s.

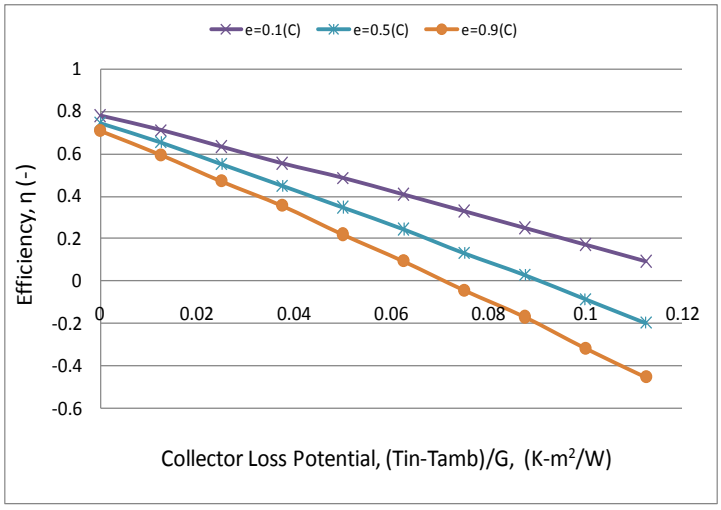

Figure 21: Total collector efficiency vs. ΔT/G at V_w=3m/s.

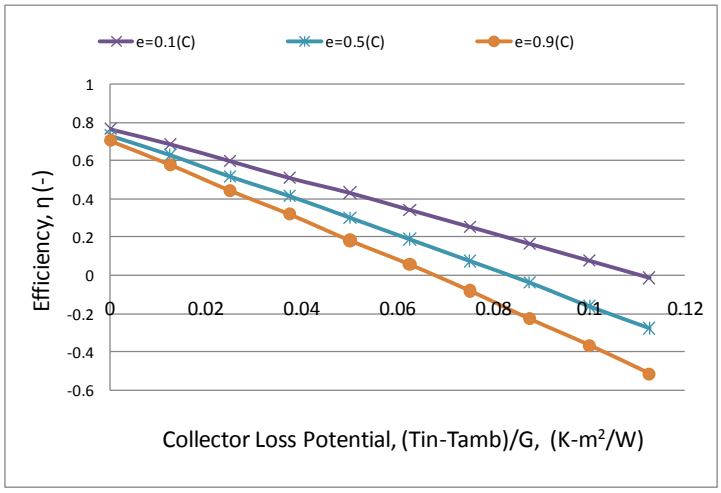

Figure 22: Total collector efficiency vs. ΔT/G at V_w=5m/s.

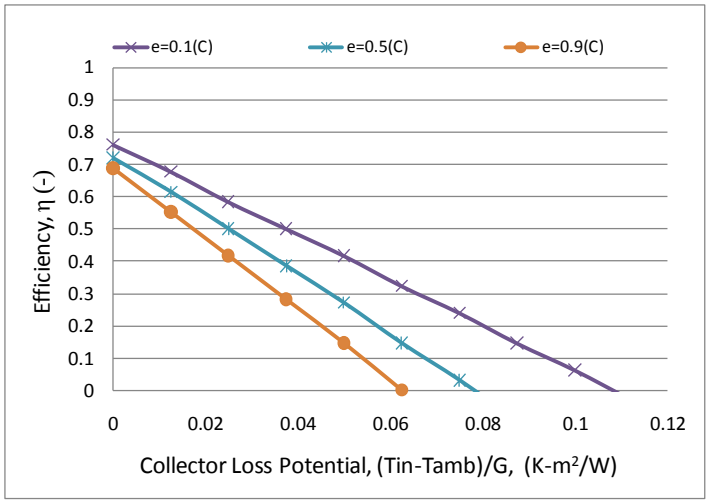

Figure 23: Collector water heating efficiency vs. ΔT/G at V_w=1m/s.

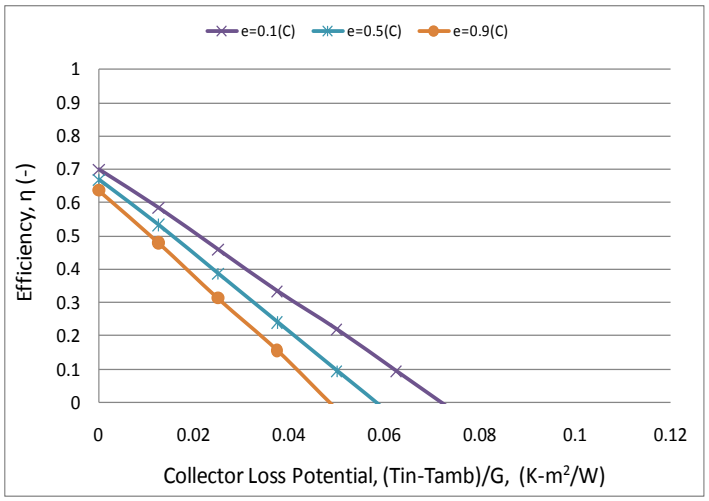

Figure 24: Collector water heating efficiency vs. ΔT/G at V_w=3m/s.

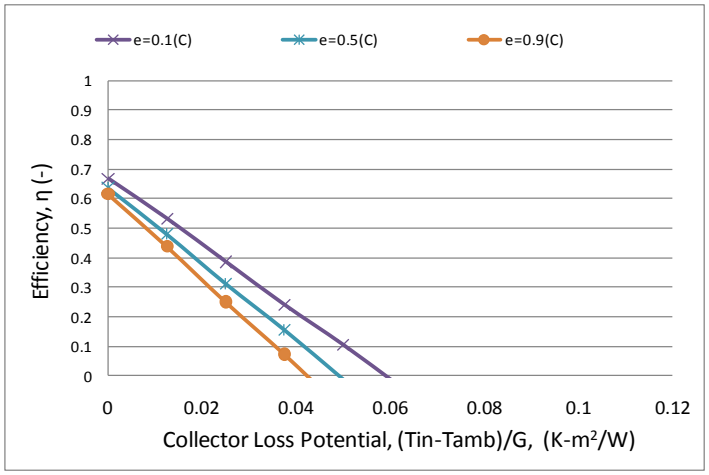

Figure 25: Collector water heating efficiency vs. ΔT/G at V_w=5m/s.

Finally a set of performance curves were obtained for wind speeds of 1m/s, 3m/s and 5m/s under varying solar radiation, G, inlet water temperature, T_{in}, and ambient temperature, T_{amb}. The values of solar radiation, inlet water temperature and ambient air temperature used as inputs to the model are given in Table 2. The performance curves for wind speeds of 1m/s, 3m/s and 5m/s are shown in Figure 26.

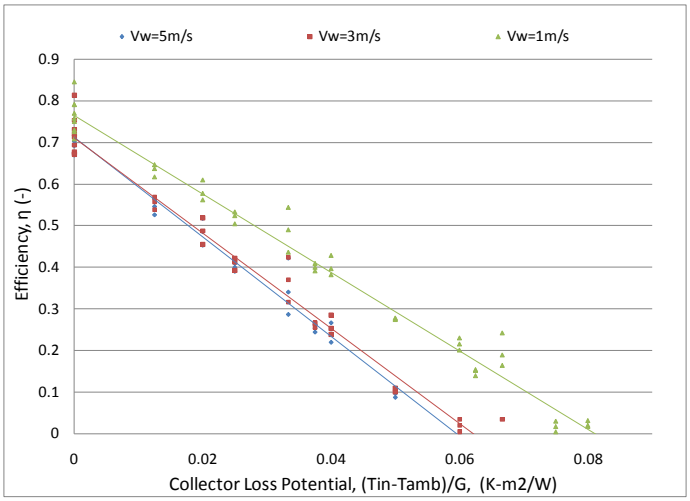

Figure 26: Total Collector efficiency vs. ΔT/G.